PHYSICAL REVIEW B VOLUME 18, NUMBER 6 15 SEPTEMBER 1978

Nonlinear electron-density distribution around point defects in simple metals. II. Applications*

P. Jena and A. K. Gupta
Physics Department and Materials Research Center, Northwestern University, Evanston, Illinois 60201

K. S. Singwi
Physics Department and Materials Research Center, Northwestern University, Evanston, Illinois 60201 and Argonne National Laboratory, Argonne, Illinois 60439

(Received 10 January 1977)

Electron distribution around point defects (vacancies, voids, and impurities) in a number of simple metals has been calculated using linear and generalized nonlinear-response theories and compared with that obtained from a self-consistent calculation based on the density-functional formalism of Hohenberg, Kohn, and Sham. Using these electron-density profiles, positron lifetimes, and angular correlation between annihilation photons in vacancies and small voids are calculated. We have also computed the distribution of electric-field gradients due to several impurities in Al. The results are compared with experiment.

I. INTRODUCTION

In the preceding paper[1], hereafter referred to as I, we have given a modification, which is exact in the limit of long wavelength, of the nonlinear theory[2] of Sjölander and Stott of electron distribution around point defects in simple metals. To test how good this theory is, we have compared the electron-density distribution around a vacancy, an eight-atom void, and a pseudoion in an electron gas of density $r_s = 2.07$ with that given by a fully self-consistent calculation based on the Kohn-Sham density-functional formalism.[3] The density profiles in all these cases have also been calculated in a linear response theory and in the original Sjölander-Stott theory. The purpose of this paper is to make use of the results of the electron-density distribution around impurities and point defects in simple metals to calculate quantities which are experimentally observable. The properties considered here are (a) characteristics of positron annihilation, such as the lifetime of positrons and angular-correlation between annihilation photons in vacancies and small metal voids, and (b) electric field gradients in cubic metal alloys. Experimental investigation in these two areas has begun during recent years and data, although scarce, are now available for comparison with theory.

This paper is divided into two main sections. In Sec. II we discuss the positron annihilation in vacancies and in small metal voids, and in Sec. III we calculate electric field gradients at Al-host lattice sites due to Mg, Ga, Ge, and Si impurities. The results are summarized in Sec. IV.

II. POSITRON ANNIHILATION IN VACANCIES AND SMALL METAL VOIDS

A. General considerations

It was first observed by McKenzie[4] that at elevated temperatures the lifetimes of positrons increased in metals. This result can be interpreted in terms of the trapping model[5] of Bergersen and Stott according to which the increased number of vacancies produced by the thermal excitation of the solid trap the positrons, which then annihilate with the inhomogeneous distribution of the electrons around the defect. And since the electron density inside the vacancy is less than the average density of the host, the lifetime of a bound positron is usually larger than that of a free positron annihilating in the bulk. Thus the positrons can be used to probe, although in an average sense, the electron density around a vacancy in solids. The same is true for a void in a metal.

The annihilation rate λ of positrons in an inhomogeneous electron gas can be written

$$\lambda = \int d\vec{r}\, |\psi^+(\vec{r})|^2 \Gamma(n(\vec{r})), \tag{1}$$

where

$$\Gamma(n) = (2 + 134\, n) \times 10^9 \text{ sec}^{-1} \tag{2}$$

is the annihilation rate for a homogeneous electron gas of density n. Formula (1) was given by Brandt[6] and is in the spirit of a local-density approximation. $\psi^+(r)$ is the wave function of the positron in the bound state and is given by

$$\psi^+(\vec{r}) = U_{nl}^+(r)/r\, Y_{lm}(\hat{r}), \tag{3}$$

where $U^+(r)$ is obtained by solving the following radial Schrödinger equation for bound states:

$$\left(-\frac{d^2}{dr^2}+V_+(r)-\frac{l(l+1)}{r^2}\right)U^+_{nl}(r)=-\epsilon^{nl}_+U^+_{nl}(r). \quad (4)$$

$V_+(r)$ and ϵ^{nl}_+ are, respectively, the effective positron-defect potential and the binding energy of the positron in the nl quantum state. The effective positron potential $V_+(r)$ is given by

$$V_+(r)=-V_0\theta(r-a)+[V^+_{\rm corr}(n(r))-V^+_{\rm corr}(n_0)]+\Phi(n(r)), \quad (5)$$

where V_0 is the zero-point energy of a positron in a perfect lattice and $V^+_{\rm corr}$ is the positron-electron correlation energy in the local-density approximation. The positron-defect electrostatic potential Φ is simply the negative of the electron-defect potential described in I. The zero-point energy has been taken from the work of Hodges and Stott[7] and the positron-electron correlation energy from the work of Bhattacharyya and Singwi[8]. a is the radius of the defect. Thus knowing $V_+(r)$ from Eq. (5), Eq. (4) can be solved numerically to compute the bound-state wave function of the positron.

The wave function of a positron in a shallow bound state extends to large distances from the defect, and, therefore, an appreciable part of the positron can annihilate with the core electrons of the host. The annihilation of positrons with electrons outside the defect radius can be taken into account by scaling the electron density outside the defect in a manner suggested by West,[9] namely,

$$n'(r)=n(r)(1+\Gamma_c/\Gamma_v), \quad (6)$$

where Γ_c and Γ_v are annihilation rates with core and valence electrons, respectively, and are estimated from angular correlation measurements:

$$\Gamma_c/(\Gamma_c+\Gamma_v)=0.8A_c/(A_c+A_v), \quad (7)$$

where A_c and A_v are experimental areas under core and valence electron parts of the angular-correlation curve, respectively.

Interesting experimental information on the electron density can also be obtained from the study of angular-correlation between two annihilation γ-ray quanta. Since the linear momentum of the thermalized positrons is small compared with the Fermi momentum of electrons, this measurement furnishes information on the distribution of electron momentum. In the independent particle model, the momentum density of the electron-positron pair is

$$\rho(\vec{p})\propto\sum_i\int d\vec{r}\,e^{-i\vec{p}\cdot\vec{r}}\,|\psi_+(\vec{r})\psi_i(\vec{r})|^2, \quad (8)$$

where $\psi_i(\vec{r})$ is the electron wave function in the occupied state i. The angular-correlation curve can then be computed from the expression

$$I(p_z)=\int_{p_z}^{\infty}dp\,p\rho(p), \quad (9)$$

where p_z is given by

$$\theta=p_z/m_0c, \quad (10)$$

θ being the angle between the two γ-ray quanta.

In order to calculate the electron charge density around a defect, we have considered two models: (1) a "hole" in a jellium and (2) pseudopotential model.

1. *Jellium model for a defect*

In this model a vacancy is created by digging a hole of radius a corresponding to the Wigner-Seitz radius. Thus small voids of radii $2a$ and $3a$ would correspond, respectively, to the removal of 8 and 27 atoms. The external potential corresponds to an ion density,

$$n_+(r)=n_0\theta(r-a), \quad (11)$$

where $n_0=Z/\Omega_0$ is the electron density of the homogeneous electron gas with Z electrons in volume Ω_0.

Electron-density profiles around a monovacancy and around 8-atom and 27-atom voids have been computed using linear and nonlinear response theory, the Thomas-Fermi (TF) model, and the density-functional formalism of Hohenberg-Kohn-Sham (HKS). Comparisons of these profiles has already been made in I. In Fig. 1 we have plotted the various contributions (Thomas-Fermi, electrostatic, and exchange-correlation) to the self-

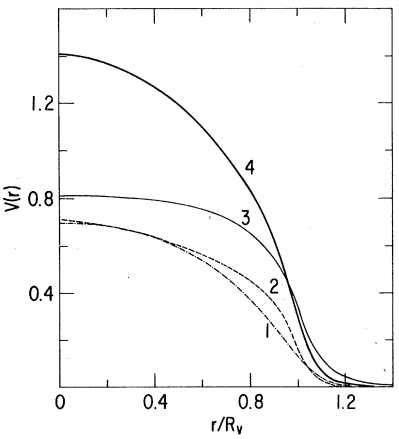

FIG. 1. The Hartree (curve 1), the exchange-correlation (curve 2), and the total effective (curve 4) electron-void potentials for a 27-atom void in Al vs r/R_v. Curve 3 is the effective potential in the Thomas-Fermi case. The potentials are in a.u. and R_v is the radius of the void.

consistent potential due to a 27-atom void in Al. Relative importance of the various terms is similar for all other sizes of the defect. It is interesting that the exchange-correlation potential is as large as the electrostatic potential. Since the exchange-correlation potential is obtained in the local-density approximation, one naturally wonders about the importance of higher-order gradient corrections to exchange-correlation energy in determining the electron-density distribution. The effect of these corrections has been studied by Jena and Singwi[10] to first order in the nonlinear screening of hydrogen in simple metals and by Gupta and Singwi[11] to second order in the calculation of surface profiles. The gradient corrections were found to be rather small. The total electron-defect potential at the origin is greater than the Fermi energy. Thus the charge densities computed in the linear response theory (where the effective potential is considered to be weak) cannot be reliable.

In Fig. 2(a) we have compared the total effective potential of an electron for a monovacancy and voids of 8 and 27 atoms in Al. Not only the range of the potential increases linearly with the defect radius, but the effective potential at the origin of the defect is larger for increasing defect size. At this point, it is interesting to compare the quantity,

$$W = V_{\text{eff}}(r=0) - E_F,$$

which is −1.85, 2.20, and 3.98 eV, respectively, for a monovacancy and 8-atom and 27-atom void in Al ($r_s = 2.07$). W in the surface problem has the

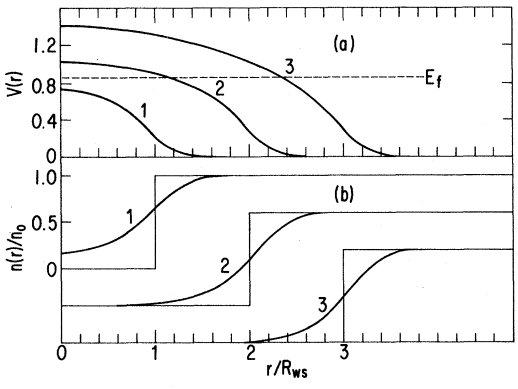

FIG. 2. (a) The electron-defect potential for a monovacancy (curve 1), and 8-atom void (curve 2), and a 27-atom void (curve 3) in Al vs r/R_{WS}. R_{WS} is the radius of a monovacancy ($R_{WS} = 2.98$ a.u.). E_f is the Fermi energy. (b) The normalized electron charge density $n(r)/n_0$ around a monovacancy (curve 1), an 8-atom void (curve 2), and a 27-atom void (curve 3) in Al vs r/R_{WS}. The curves have been displaced with respect to each other vertically for clarity.

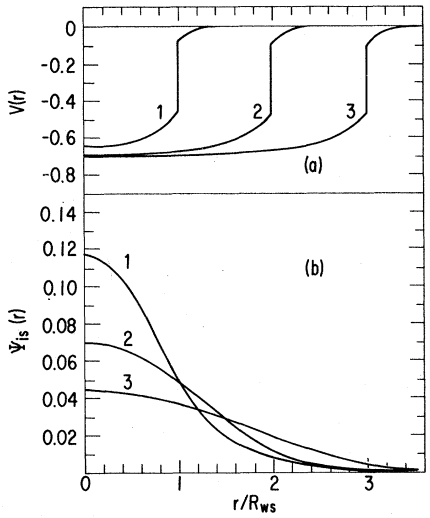

FIG. 3. (a) The positron-defect potential for a monovacancy (curve 1), an 8-atom void (curve 2), and a 27-atom void (curve 3) in Al vs r/R_{WS}. (b) The 1s bound-state positron wave function $\psi_{1s}(r)$ in a monovacancy (curve 1), an 8-atom void (curve 27), and a 27-atom void (curve 3) in Al vs r/R_{WS}.

significance of a work function. Lang and Kohn's value[12] of W for $r_s = 2$ is 3.89 eV.

In Fig. 2(b) the electron-density distribution normalized to the average density of Al metal is plotted for three sizes of the defect. It is interesting to note that $n(r)/n_0$ is about 0.2, 0.01, and 0 for a monovacancy and for 8-atom and 27-atom voids, respectively, indicating that the strength of the potential increases with the size of the defect. Furthermore, the electron-density profile near the surface of the defect gets increasingly sharper as the defect gets bigger. Comparison with the calculations of Lang and Kohn[13] for a jellium of $r_s = 2$ indicates that for a void of radius 10 Å or more, the electron profile for all practical purposes, would resemble that for a surface.

To calculate the positron-annihilation characteristic, we have first computed the effective positron-defect potential using the self-consistent electron density in the absence of a positron from Eq. (5). The results for Al are shown in Fig. 3(a). There are two main features to be noted. The positron-defect potential is attractive and its strength increases with the defect size. Secondly, the potential seen by a positron is maximum attractive at the center of the defect implying that the positron would prefer to reside at the center of the void. However, as the voids become very large, considerations of image potential could influence this situation.

With this positron potential, we have solved the Schrödinger equation (4) for negative energy states

TABLE I. Positron bound states and lifetimes in a monovacancy, 8-atom void and 27-atom void in Al.

Size of the defect	Bound state	Binding energy (eV)	Lifetimes (psec)
Monovacancy	1s	−1.75	243
8-atom void	1s	−6.31	399
	2s	−0.07	210
27-atom void	1s	−7.87	465
	2s	−3.91	386
	2p	−1.52	331

to locate the existence, if any, of bound states. The quantum states of the bound positron along with the corresponding binding energies are given in Table I. It is seen that the positron potential for larger defects becomes strong enough to bind more than one positron, the positrons with higher binding energies becoming more localized. Lifetimes of positrons in these bound states are computed using the positron wave function in respective bound states from Eq. (1). The results are given in Table I.

Although there are multiple bound states, because of the low flux the positron would always prefer to go into the lowest bound state. It is for this reason that in Fig. 3(b) we have plotted the positron wave function in the 1s bound state for three defect sizes. We find that while 35% of the positrons lie outside the vacancy radius, only 5% and 1% of the positrons lie outside the radius of 8- and 27- atom voids, respectively. Thus the effect of core electrons on positron annihilation rate plays an insignificant role in voids. The calculated lifetime of positrons (in Table I) in a monovacancy is in good agreement with experiment. Unfortunately, lifetimes of positrons in small Al voids are not yet available. When small voids of controlled size could be produced, it would be interesting to check our theoretical values against experiment.

It is, however, interesting to note that the lifetime of positrons increases markedly with the increase in the size of a void. This is an important observation since it links the size of small voids to the positron life. Positron annihilation characteristics can therefore be used to monitor the nucleation and growth of small voids where conventional electron microscopy is found to be inadequate. For large voids, the positron lifetime as computed from Eq. (1) would tend to saturate to a value of 500 psec (spin-averaged positronium lifetime). The use of the Brandt-Reinheimer formula[6] to compute the positron lifetime in the inhomogeneous electron gas implies that the positronium would be formed in large metal voids. Although there is fragmentary experimental evidence[14,15] that the trapped state in large voids has some positroniumlike properties, and recent calculations indicate[16] that such a state is energetically favorable, experiments done under strong magnetic fields[17] fail to show any sign of positronium formation. MacKenzie and Sen[18] have recently cautioned their readers against using the later experimental result as conclusive evidence that positroniumlike states are not possible in large metal voids.

For very large voids (mean diameter 40 Å) lifetimes up to 595 psec have been measured by Cotterill *et al.*[17] in irradiated molybdenum. Recently, Cheng *et al.*[19] have measured positron lifetimes in voids of molybdenum by varying the temperature and dosage of irradiation and they found that the lifetimes saturated to a value of about 453 psec. The discrepancy between these two sets of data in molybdenum is now believed to be due to the presence of impurities around which vacancies tend to cluster to form voids.

As shown earlier, the electron-density profile at the internal surface of voids (whose diameter $\gtrsim 20$ Å) resembles closely that of a metal vacuum surface. Thus for voids as large as 20 Å in diameter, the image potential would form a major fraction of the positron trapping potential in Eq. (5). Calculations[20] show that positrons are trapped at internal surfaces of large metal voids. Thus for voids whose internal surfaces resemble metallic surfaces, the positron lifetime would be smaller than 500 psec (spin-averaged positronium lifetime) not only because the electron densities in the region of void surface are bigger than those in the center, but the core electrons of the host ions would participate in the annihilation process. The relative importance of image potential as a function of void size is an interesting problem for a future study since it would provide an understanding of how positron lifetime behaves as we approach the critical size at which the void resembles a surface.

In Fig. 4 we present the angular-correlation curves normalized to equal areas for a monovacancy, an 8-atom void, and a 27-atom void in arbitrary units. We find that the full widths at half-maximum (FWHM) of these curves are 8.8, 7.3, and 6.5 mrad, respectively. Trifthäuser *et al.*[14] have measured the angular-correlation curves in a monovacancy and in a large void in Al. Experimental values of FWHM for a monovacancy and a large void are, respectively, 8.8 and 6.5 mrad, which are in good agreement with our calculated values. Not much significance can be attached to the agreement of FWHM between theory and experiment for a large void,

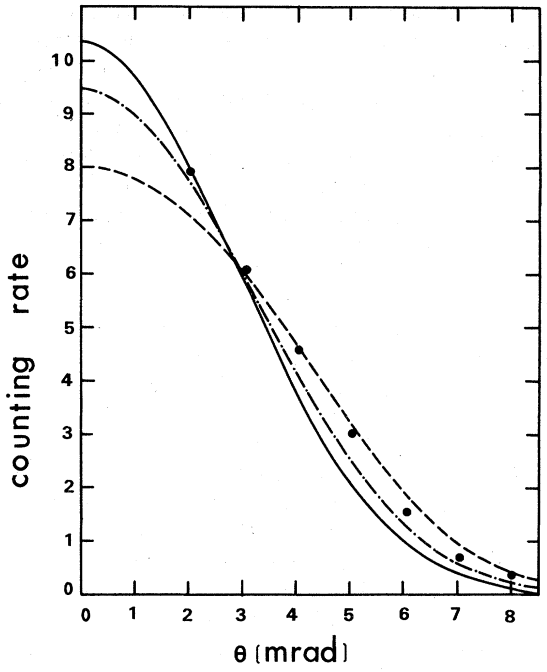

FIG. 4. The angular-correlation curve for a monovacancy (dashed curve), an 8-atom void (dash-dot-dash curve), and a 27-atom void (solid curve) in Al vs θ(mrad). All of the curves have been normalized to the same area. The vertical scale is in arbitrary units. Experimental points from Ref. 15 are shown as solid do+

since we have not considered surface trapping. However, the narrowing of the peak of the angular correlation curves with the size of the void is consistent with experimental data[14] in Al. The decrease in FWHM with increasing size of the void in molybdenum[21] is also consistent with our results in Al, although the broadening of the angular-correlation peak[17, 22] with increasing void diameter still remains a puzzling result.

Using the jellium model, Manninen *et al.*[23] have computed the lifetimes of positrons in a large number of metal vacancies using both HKS and TF methods for the calculation of $n(r)$. In the following, we describe another model of a vacancy in simple metals—the pseudopotential model.

2. *Pseudopotential model for a vacancy*

In this model, the electron Hamiltonian for the solid is written

$$H_0 = T + \sum_v w(r - R_v), \tag{12}$$

where T is the kinetic energy of the electron and the total electron-lattice potential is assumed to be a linear superposition of the electron-ion pseudopotential w, centered at each ion site R_v. A vacancy is created by removing one such pseudopotential from the origin. Thus the total Hamiltonian containing one vacancy at $R_v = 0$ is

$$H = T + \sum_v{}' w(r - R_v) = H_0 - w(r). \tag{13}$$

The response of the conduction electrons to such an external potential is obtained by treating the pseudopotential nonperturbatively within the framework of the generalized nonlinear response theory for a two-component plasma, described in I.

We have used the model pseudopotential of Animalu and Heine[24] as tabulated by Harrison.[25] To eliminate the large unphysical oscillations in the pseudopotential form factors $w(q)$ for large q we have used a cutoff factor $\exp[-0.03(q/2k_F)^{12}]$. Such a cutoff produced pseudopotential form factors that agree well with those determined empirically and are essentially zero for $q/2k_F > 1.5$.

We have then extracted the bare-ion pseudopotentials $w_b(q)$ by descreening the Animalu-Heine form factors through use of the Hubbard dielectric constant since it was used in the calculation of Animalu and Heine. In real space, the bare-ion potential for the vacancy in the jellium model is found to be maximum repulsive at the center of

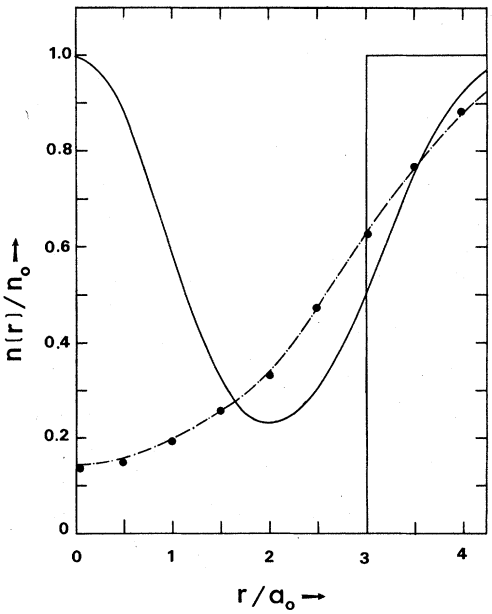

FIG. 5. The normalized electron density $n(r)/n_0$ around an Al vacancy in two different models vs r/a_0. The solid curve corresponds to the pseudopotentials model of the vacancy. The dot-dash curve corresponds to a "spherical-hole" in the jellium model. The solid dots are the results of Kohn-Sham calculation for a spherical-hole model.

the vacancy, while in the pseudopotential model, the potential is maximum repulsive for the electron at the surface of the pseudoion core.

To appreciate the influence of these potentials on the distribution of conduction electrons around the vacancy, we have plotted $n(r)/n_0$ for Al in Fig. 5 for these two models. While for a jellium model the maximum number of electrons are repelled from the center of the vacancy, in the pseudopotential model the maximum number of the electrons are repelled from a region around the radius of the pseudoion core. This behavior is a manifestation of the precise form of bare-ion potentials mentioned earlier.

In order to calculate the positron lifetimes in vacancies in the pseudopotential model, we again need to know the positron wave function. For this purpose, we have replaced the positron-defect potential by a square-well of radius a of the defect. Such an approximation is not unreasonable in view of the positron-defect potential presented in Fig. 3(a). The depth of the square well is then chosen so that it reproduces the binding energy of positrons in metals given by Hodges and Stott. We find that the positron lifetimes are not sensitive to the precise choice of the positron well depth. Using the positron wave function thus computed from a square-well model and the electron density in the mean-field approach, we have calculated the positron lifetimes from Eq. (1). The results are given in Table II for several simple metals and are compared with the jellium calculations of Manninen *et al.*[23] Although the electron densities in both the jellium and pseudopotential models are very different, the lifetimes in the two models compare favorably with each other. Since the positron annihilation rate is an integrated quantity, it is not very sensitive to the precise nature of the electron distribution. The results are in semiquantitaive agreement with experimental values in Table II.

B. Effect of lattice relaxation

It is to be noted that our computed positron lifetimes in metal vacancies are generally larger than the experimental values. So far we have neglected the effect of lattice relaxation around a vacancy on the positron lifetime. Although this is difficult to treat from first principles, we can estimate its effect by following the prescription of Blatt[26], who suggested that the charge Z corresponding to a pseudoion due to lattice relaxation reduces by the same amount the volume contracts. In other words,

$$Z^*/Z_0 = \Omega/\Omega_0,$$

where Z_0 and Ω_0 are the valence and volume per atom in the unperturbed state. Ω is the volume occupied by the vacancy after lattice relaxation and Z^* is the charge contained in the relaxed vacancy. Thus we have taken this effect into consideration by reducing the strength of the bare-ion pseudopotential by Ω/Ω_0 and repeating

TABLE II. Positron lifetimes in monovacancies of metals in point-ion model.

	Lifetimes in psec				
		Pseudopotential model		Jellium model without relaxation (Ref. 23)	
Metal	Expt.	With relaxation	No relaxation		% e^+ inside vacancy
Na	338[a]	389	405	391	32
Cs	418[a]	433	462	452	41
Mg	255[b]	277	315	307	57
Zn	240[c]	224	249	233	56
Cd	232[c]	250	277	276	51
Al	243[d]	204	243	237	65
Ga	260[e]	210	249	248	57
In	240[f]	235	302	289	61
Tl	230[b]	247	313	302	56
Pb	274[b]	258	304	291	62

[a] I. K. MacKenzie, T. W. Craig, and B. T. A. McKee, Phys. Lett. A 36, 227 (1971).
[b] B. T. A. McKee (unpublished).
[c] I. K. MacKenzie, T. L. Khoo, A. B. McDonald, and B. T. A. McKee, Phys. Rev. Lett. 19, 946 (1967).
[d] T. M. Hall, A. N. Goland, and C. L. Snead, Jr., Phys. Rev. B 10, 3062 (1974).
[e] W. Brandt and H. F. Waung, Phys. Lett. 27A, 700 (1968).
[f] V. H. C. Crisp, D. G. Lock, and R. N. West, J. Phys. F 4, 830 (1974).

the calculation of both $n(r)$ and the positron wave function.

The results are compared with experimental values in Table II. Since the external potential due to lattice relaxation is now weaker, the electron density $n(r)$ does not deviate from n_0 as strongly as that in the unrelaxed case. This causes the lifetime to decrease, a result that brings theory into better agreement with experiment.

The results in alkali metals deserve some special consideration, since the measured lifetimes of positrons in vacancies are found to be almost the same as those in perfect metals, whereas the theoretical values even including lattice relaxation effects indicate that the lifetimes in vacancies should be higher than those in the bulk. To understand this anomalous behavior we note that for the lifetime of positrons in vacancies and bulk to be different, the following three conditions have to be satisfied: (i) The positron should be bound to the vacancy, (ii) the trapping rate of positrons should exceed the annihilation rate, and (iii) the rate of escape of positrons from the bound state should be less than the annihilation rate.

The first two conditions are satisfied for all metals we have studied. In alkali metals, the positrons lie in a very shallow bound state with binding energy of 0.01 eV. In order to estimate the frequency ν with which the positrons knock on the vacancy wall, we make use of the uncertainty relation, $\Delta x \cdot \Delta p \simeq \hbar$. Taking Δx to be the Wigner-Seitz radius of the vacancy, we estimate this frequency in Na to be 3.54×10^{14} sec^{-1}. Thus the escape rate given by $e^{-\Delta E/kT}\nu$ (where ΔE is the binding energy, 0.01 eV) is 6×10^{12} sec^{-1}. This is much larger than the annihilation rate, which is typically 3×10^{9} sec^{-1}. Thus in alkali metals the positrons escape the vacancy before they have an opportunity to annihilate with the inhomogeneous distribution of electrons. This qualitatively explains the anomalous positron annihilation characteristics in alkali metals.

We now turn to the discussion of electric field gradients in cubic metal alloys that provides information on the large r behavior of the electron charge density.

III. ELECTRIC FIELD GRADIENTS IN CUBIC METAL ALLOYS

The rapid loss of intensity of nuclear-magnetic-resonance (NMR) signals in cubic metal alloys has been attributed to the interaction of the nuclear quadrupole moment of the host nucleus with the electric field gradients produced by impurities at the host sites. It is well known that the electric field gradients (efg) at a nuclear site in a cubic metal vanish due to symmetry considerations. However, introduction of impurities destroys this cubic order and gives rise to electric field gradients that extend as far as the fifth neighbor sites. Experiments[27] on both powder and single crystals have been performed and electric field gradients at several host sites due to various impurities determined.

The theory of the origin of the efg has been discussed by both Bladin and Friedel[28] and Kohn and Vosko.[29] They show that for a single impurity the asymptotic form for the efg distribution around the impurity can be written

$$eq(r) = \tfrac{8}{3}\pi\, e\alpha(\vec{k}_F)\Delta n(r), \tag{14}$$

where $\alpha(\vec{k}_F)$ is the so-called Bloch enhancement factor,[30]

$$\alpha(\vec{k}_F) = \int d\vec{r}\,\psi^2_{k_F}(\vec{r})\,\frac{[1+\gamma(r)]P_2(\cos\theta_{k_F}r)}{r^3} \times \left(\int d\vec{r}\, e^{2i\vec{k}_F\cdot\vec{r}}\,\frac{P_2(\cos\theta_{k_F}r)}{r^3}\right)^{-1}. \tag{15}$$

$\psi_{k_F}(\vec{r})$ is the Bloch wave function for the host conduction electrons, $\theta_{k_F}r$ is the angle between $\vec{k}_F$ and $\vec{r}$, and $\gamma(r)$ is the Sternheimer antishielding factor.[31] $\Delta n(r)$ is the difference between the electron-density distribution around the impurity ion in the host lattice and around the host ion, namely,

$$\Delta n(r) = n_{\text{IMP}}(r) - n_{\text{host}}(r). \tag{16}$$

Note that the Bloch enhancement factor in Eq. (2) is independent of the impurity potential and depends only on the band structure of the host. The difference in the charge density, $\Delta n(r)$ is, however, strongly dependent on the nature of the impurity.

Recently, Stiles and Williams[32] have studied the efg due to Mg, Ga, Ge, and Si in Al and measured the field gradients up to four near-neighbor sites. They obtained the striking result that the efg at the second near-neighbor site due to all these impurities are small. Assuming that this may be due to the property of the host, Holtham and Jena[30] carried out a full band-structure calculation of the anisotropy of the Bloch enhancement factor, $\alpha(\vec{k}_F)$ with $\vec{k}_F$ along [110] (first neighbor), [100] (second neighbor), [211] (third neighbor), and [111] (fourth neighbor) directions. They found that although $\alpha(\vec{k}_F)$ along the second-neighbor direction is small by about 20% of that along first, third, and fourth neighbor directions, the enhancement was not small enough to explain the experimental data.

Fukai and Watanabe[33] have calculated $\Delta n(r)$ using Ashcroft pseudopotential[34] and linear-response theory as outlined in I. Using the values of $\alpha(\vec{k}_F)$

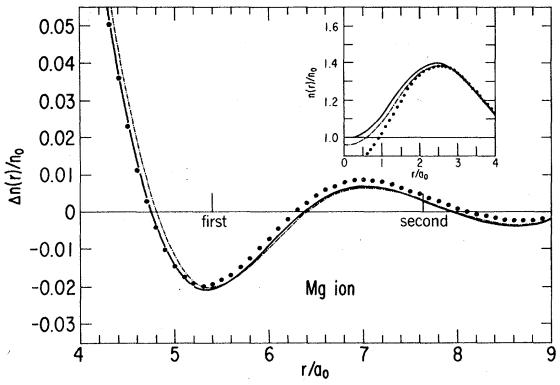

FIG. 6. The displaced electron-density distribution $n(r)/n_0$ surrounding a Mg ion placed in a jellium corresponding to Al metal ($r_s = 2.07$) vs r/a_0. The indent shows the charge distribution near the impurity ion while the Friedel oscillations in the screening charge density are shown on a magnified scale. The solid line is the result of a nonlinear self-consistent calculation, while the dot-dash line is the result of the linear-response theory. The solid dots represent the results of the self-consistent Kohn-Sham calculation. The positions of the first and second near-neighbors of the impurity are also shown.

of Holtham and Jena and the linear-response result for $\Delta n(r)$ from the work of Fukai and Watanabe, one finds that the theoretical estimate of $eq(r)$ is as much as an order of magnitude smaller than the experimental value. This discrepancy could be due to two main reasons: (i) The theory of Bladin and Friedel and Kohn and Vosko is inadequate to treat the efg problem even for the first four neighbor sites or (ii) the charge-density distributions around the impurity and host ions in the linear-response theory are not reliable.

We have already emphasized that the charge-density distribution around pseudoions in the nonlinear response theory is very different from that of the linear-response theory. It is therefore imperative that a full nonlinear-response calculation of the charge density around impurities in Al be carried out to determine the electric field gradients. Comparison of these theoretical results with experiment would then yield reliable information regarding the validity of the existing theories of efg in dilute cubic metal alloys.

Using the bare-ion model potentials with appropriate cutoff factor (described earlier), we have calculated the electron-density distribution around Mg, Ga, Ge, Si, and Al ions immersed in a jellium of $r_s = 2.07$ (Al density) in linear-response theory, nonlinear-response theory for a two-component plasma and the density-functional formalism of Kohn and Sham as described in I. To illustrate the differences in charge densities in these formulations, we have plotted $n(r)/n_0$ around Mg, Al, and Ge in Figs. 6, 7, and 8, respectively.

The electron densities in nonlinear-response theory without density derivative terms are found to differ considerably both in magnitude and phase and are not shown in the figures for comparison. While the nonlinear-response results with the density-derivative term are closer to the linear-response theory, both these charge densities differ considerably from the Kohn-Sham result. Most likely reasons for this are already discussed in I and will not be repeated here.

Using the Bloch enhancement factors, $\alpha(\vec{k}_F)$ of Holtham and Jena, we have presented in Table III the electric field gradients up to the first four Al-neighbor sites due to Mg, Ga, Ge, and Si impurities. It is surprising that as far as comparison of calculated efg with experiment is concerned, there does not seem to be much difference between linear and nonlinear results. We shall comment on this in Sec. IV.

Vacancies in Al can also be regarded as impurities that can give rise to efg at Al sites. Our estimation of $eq(r)$ at the first Al neighbor site due to a vacancy using the calculated densities in the Kohn-Sham formulation is -7.0×10^{13} cgs esu.

In our calculation, the effect of lattice distortion —a quantity whose magnitude is difficult to estimate,—has been neglected. Carbotte[35] has estimated that due to Mg impurity in Al, the first neighbors move outward by 2%. This small displacement would cause the first-neighbor efg to change from −18.4 to −18.0 (using our Kohn-Sham values).

IV. SUMMARY AND CONCLUSION

We have calculated electron-density distribution around monovacancies, voids and impurities in

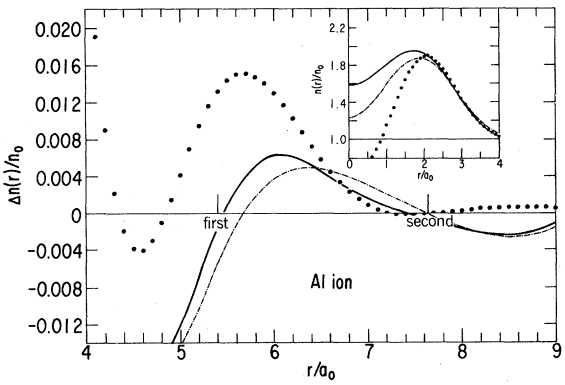

FIG. 7. The displaced electron-density distribution $n(r)/n_0$ around an Al ion placed in a jellium corresponding to Al metal vs r/a_0. The rest of the legend is the same as that for Fig. 6.

TABLE III. Electric field gradient in 10^{13} cgs esu at host neighbor site in Al alloys.

Impurity	Neighbor location	$eq(r)$ Linear response	$eq(r)$ Nonlinear response	Kohn-Sham	| Expt. | (Ref. 32)
Mg	1	−8.4	−11.1	−18.4	9.2
	2	+1.4	+1.7	+2.2	0
	3	−0.3	−0.5	−0.6	3.1
Ga	1	+4.2	+5.9	+5.8	10.8
	2	−2.3	−2.6	−2.6	
	3	+0.9	+0.8	+0.8	
Ge	1	+8.6	+9.9	+9.8	15.5
	2	−1.2	−1.3	−0.5	2.2
	3	+1.0	+1.1	+0.2	3.8
Si	1	+3.6	+5.0		13.3
	2	+1.0	+0.9		
	3	+2.5	+2.6		2.8

several simple metals both in the linear- and nonlinear-response theories, and have compared these results with those obtained from a fully self-consistent calculation based on Kohn-Sham scheme. We find that there is a considerable difference in both magnitude and phase between the results of linear and nonlinear theories. The inescapable conclusion is then that even for the so called "weak" pseudopotential, the linear-response results are not very reliable.

As regards positron lifetimes in monovacancies, the agreement between simple theory and experiment is reasonable. To obtain a more quantitative agreement, the influence of positrons on the electron-density distribution and the effect of lattice relaxation around the vacancies must be considered. The former can be treated within the modified Sjölander-Stott scheme but at the expense of considerable numerical work. Being an average quantity, the positron lifetime does not depend on the precise electron-density distribution and as such cannot be used to probe the latter.

Concerning the electric field gradients in cubic metal alloys, the results are found to be very sensitive to the precise form of $\Delta n(r)$, which in turn depends upon the nature of the pseudopotential for the host and impurity ions. For example, as mentioned earlier, using Ashcroft pseudopotentials and linear-response theory, the computed electric field gradients are about an order of magnitude smaller than experiment. On the other hand, using still the linear-response theory and Heine-Aberenkov model potentials with appropriate cutoff factors, one gets a more reasonable agreement with experiment in Table II. While there does not seem to be a clear distinction between linear- and nonlinear-response results for $eq(r)$ in Table II, the near similarity must be regarded as fortuitious in view of our results in Figs. 6, 7, and 8. The effect of lattice displacement around impurities could be important. The contribution to $eq(r)$ caused by lattice strain is not included in our present calculation. Thus we feel that with a proper choice of pseudopotential and, perhaps, lattice displacement effects, it should be possible to achieve agreement between theory and experiment. The theories of Kohn-Vosko and Blandin-Friedel give reasonable description of the electric field gradients in cubic metal alloys. The separation of the efg into a Bloch enhancement factor (a solid-state effect) and the response of a nearly-free-electron system seem to be reasonable for distances as close as the first-neighbor site.

So far our calculations have been done in the

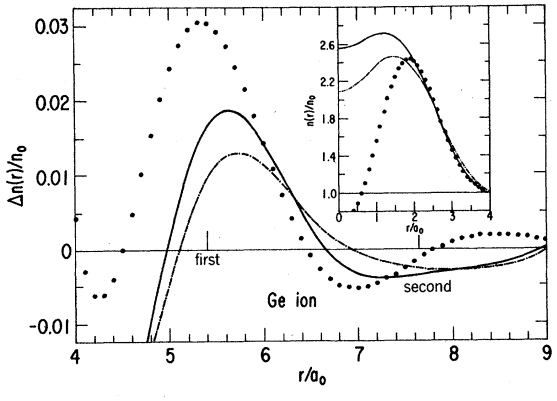

FIG. 8. The displaced electron density distribution $n(r)/n_0$ around a Ge ion placed in the jellium corresponding to Al metal vs r/a_0. The rest of the legend is the same as that for Fig. 6.

jellium approximation for the solid. The periodic arrangement of ions in a solid is expected to modify the calculated electron-density distributions. This effect can be incorporated, without too much difficulty, within the spherical solid model introduced by von Barth and Ambladh.[36] It could lead to significant changes in the calculated efg but is not expected to modify positron lifetimes.

---

*Work supported by the NSF through Northwestern University Material Research Center and NSF Grant No. DMR73-07659.

[1]A. K. Gupta, P. Jena, and K. S. Singwi, preceding paper, Phys. Rev. B 18, 2712 (1978).
[2]A. Sjölander and M. J. Stott, Phys. Rev. B 5, 2109 (1972).
[3]P. Hohenberg and W. Kohn, Phys. Rev. 136, B864 (1964); W. Kohn and L. J. Sham, Phys. Rev. 140, A1133 (1965).
[4]I. K. MacKenzie, Phys. Lett. A 30, 115 (1969).
[5]B. Bergersen and M. J. Stott, Solid State Commun. 7, 1203 (1969).
[6]W. Brandt and J. Reinheimer, Phys. Lett. A 35, 109 (1971).
[7]C. H. Hodges and M. J. Stott, Phys. Rev. B 7, 73 (1973).
[8]P. Bhattacharya and K. S. Singwi, Phys. Rev. Lett. 29, 22 (1972).
[9]R. N. West, Solid State Commun. 9, 1417 (1971).
[10]P. Jena and K. S. Singwi, Phys. Rev. B (to be published).
[11]A. K. Gupta and K. S. Singwi, Phys. Rev. B 15, 1801 (1977).
[12]N. D. Lang and W. Kohn, Phys. Rev. B 3, 1215 (1971).
[13]N. D. Lang and W. Kohn, Phys. Rev. B 1, 4555 (1970).
[14]W. Triftshaüser, J. D. McGervey, and R. W. Hendricks, Phys. Rev. B 9, 3321 (1974).
[15]P. Sen, L. J. Cheng, and H. E. Kissinger, Phys. Lett. A 53, 299 (1975); D. R. Gustafson and G. T. Barnes, J. Nucl. Mater. 48, 79 (1973).
[16]R. M. Nieminen and C. H. Hodges, Solid State Commun. 18, 1115 (1976).
[17]R. M. J. Cotterill, I. K. MacKenzie, T. G. Smedskgaer, G. Trumpy, and J. H. Traft, Nature 239, 99 (1972).
[18]I. K. MacKenzie and P. Sen, Phys. Rev. Lett. 37, 1296 (1976).
[19]L. J. Cheng, P. Sen, I. K. MacKenzie, and H. E. Kissinger, Solid State Commun. 20, 953 (1976).
[20]C. H. Hodges and M. J. Stott, Solid State Commun. 12, 1153 (1973).
[21]I. K. MacKenzie (private communication).
[22]O. Mogerson, K. Petersen, R. M. J. Cotterill, and B. Hudson, Nature 239, 97 (1972).
[23]M. Manninen, R. Nieminen, P. Hautojarvi, and J. Arponen, Phys. Rev. B 12, 4012 (1975).
[24]A. O. E. Animalu and V. Heine, Philos. Mag. 12, 1249 (1965).
[25]W. A. Harrison, *Pseudopotentials in the Theory of Metals* (Benjamin, New York, 1966), p. 310.
[26]F. J. Blatt, Phys. Rev. 108, 285 (1957).
[27]M. Minier, Phys. Rev. 182, 437 (1969).
[28]A. Blandin and J. Friedel, J. Phys. Radium 21, 689 (1960).
[29]W. Kohn and S. H. Vosko, Phys. Rev. 118, 912 (1960).
[30]P. M. Holtham and P. Jena, J. Phys. F 5, 1649 (1975).
[31]R. M. Sternheimer, Phys. Rev. 95, 736 (1954).
[32]J. Stiles and D. L. Williams, J. Phys. F 4, 2297 (1974).
[33]Y. Fukai and K. Watanabe, Phys. Rev. B 2, 2353 (1970).
[34]N. W. Aschcroft, Phys. Lett. 23, 48 (1966).
[35]J. P. Carbotte (private communication).
[36]C. O. Almbladh and U. von Barth (unpublished).